Evidence for intergranular tunnelling in polyaniline passivated α-Fe nanoparticles

2006 Nanotechnology 17 4765

(http://iopscience.iop.org/0957-4484/17/18/039)

INSTITUTE OF PHYSICS PUBLISHING NANOTECHNOLOGY
Nanotechnology **17** (2006) 4765–4772 doi:10.1088/0957-4484/17/18/039

Evidence for intergranular tunnelling in polyaniline passivated α-Fe nanoparticles

Vijutha Sunny[1], T N Narayanan[1], U S Sajeev[1], P A Joy[2], D Sakthi Kumar[3], Yasuhiko Yoshida[3] and M R Anantharaman[1,4]

[1] Department of Physics, Cochin University of Science and Technology, Cochin-682 022, India
[2] Physical Chemistry Division, National Chemical Laboratory, Pune-411 008, India
[3] Bio-Nano Electronics Research Centre, Department of Applied Chemistry, Toyo University, Japan

E-mail: mraiyer@gmail.com

Received 4 July 2006, in final form 15 August 2006
Published 1 September 2006
Online at stacks.iop.org/Nano/17/4765

Abstract
Nanoparticles are of immense importance both from the fundamental and application points of view. They exhibit quantum size effects which are manifested in their improved magnetic and electric properties. Mechanical attrition by high energy ball milling (HEBM) is a top down process for producing fine particles. However, fineness is associated with high surface area and hence is prone to oxidation which has a detrimental effect on the useful properties of these materials. Passivation of nanoparticles is known to inhibit surface oxidation. At the same time, coating polymer film on inorganic materials modifies the surface properties drastically. In this work a modified set-up consisting of an RF plasma polymerization technique is employed to coat a thin layer of a polymer film on Fe nanoparticles produced by HEBM. Ball-milled particles having different particle size ranges are coated with polyaniline. Their electrical properties are investigated by measuring the dc conductivity in the temperature range 10–300 K. The low temperature dc conductivity (I–V) exhibited nonlinearity. This nonlinearity observed is explained on the basis of the critical path model. There is clear-cut evidence for the occurrence of intergranular tunnelling. The results are presented here in this paper.

(Some figures in this article are in colour only in the electronic version)

1. Introduction

Recently, as an essential component of nanotechnology, materials consisting of particles with lower dimensions have attracted a great deal of attention. Owing to their nanometric size, these particles exhibit dramatic changes in physical and chemical properties [1–3], which could be utilized in many important applications. The demand for smaller materials for high density storage media is one of the fundamental motivations for the fabrication of nanoscale magnetic materials. The efforts to understand the physics of these smaller structures have been propelled by attempts to exploit their beneficial properties. The increased surface area and tailored surface chemistry of magnetic metal nanoparticles lead to improved magnetic as well as electrical properties. Iron, cobalt and nickel belonging to the 3d transition series are commercially important magnetic materials. They all exhibit ferromagnetic properties and are widely used in various devices. Their alloys are also extensively used for various applications. Ultrafine particles of these materials are sought after because their loop parameters can be controlled. Moreover modified iron nanoparticles can be potential materials for drug targeting and magnetic hyperthermia. However fineness also introduces further problems like oxidation. It is also known that size effects play a major role in deciding the electrical and magnetic properties of these elements. Several synthetic techniques have been

[4] Author to whom any correspondence should be addressed.

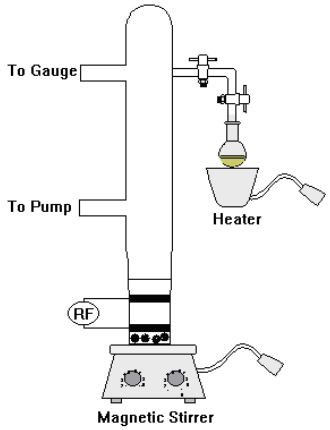

Figure 1. RF plasma polymerization set-up for surface modification of nanoparticles.

applied to synthesize magnetic metal nanoparticles, including thermal and sonochemical decomposition of organometallic precursors, high temperature reduction of metal salts and reduction with reverse micelles [4–6]. Some research groups have employed laser ablation methods and prepared magnetic nanoparticles of 40–500 atoms. However, these nanoparticles were not stable in air due to oxidation and aggregation because their surfaces were not passivated by other organic or inorganic molecules. In particular, anisotropic magnetic nanoparticles are expected to exhibit interesting magnetic properties because of the shape anisotropy. Only a few systems consisting of anisotropic magnetic nanoparticles have been developed so far.

Because of their large surface area, nanoparticles are prone to oxidation and are rendered useless as far as applications are considered. Hence they are to be passivated appropriately. The method of plasma polymerization is an inexpensive technique for producing homogeneous pin hole free films on various substrates. This method employs dc, ac and rf techniques to produce plasma. The method of plasma polymerization operates at 13.56 MHz and is widely employed for the polymerization of various monomers like aniline and pyrrole. A home-made rf plasma polymerization set-up was modified and employed for the passivation of these ultrafine powders making good use of the magnetic properties of the particles to be coated.

Mechanical attrition is a top down approach for reducing particle dimensions. High energy ball milling (HEBM) is a very convenient method for producing fineness. Particles of various sizes can be produced by controlling the time of milling and speed of attrition [7–9]. They can be then coated with polymer thin film by the method of rf plasma polymerization. However, metallic particles when passivated by insulating or semiconducting ultrathin polymer coatings exhibit altogether different magnetic and electric characteristics. Needless to say, thin coatings on the surface modify the magnetic properties; they also modify the electric properties drastically. Under such circumstances they no longer exhibit metallic characteristics; instead they display altogether different nonlinear behaviour. The nonlinearity can be a result of various factors, namely the particle size, shape, temperature or structure of the particle. The exact nature of the conduction in passivated iron nanoparticles is of interest from a fundamental point of view too. The nonlinearity in the electrical properties can be gauged by evaluating the I–V characteristics at different temperatures for different particle sizes. We endeavour in this investigation to delve into these phenomena and apply an appropriate model for the modified electrical characteristics and correlate the results. Fine powders of Fe were purchased and further ball milled in a high energy ball milling unit to reduce their particle size. Later α-Fe particles were passivated with a fine coating of polyaniline thin film [10, 11] using the modified RF plasma polymerization set-up. The changes in dc conductivity with particle size as well as coating for α-Fe have been investigated in the temperature range 10–300 K. We present a simple modified set-up based on RF plasma polymerization for passivation of magnetic nanoparticles.

2. Experimental methods

2.1. High energy ball milling

α-Fe powder was purchased from Laboratory Rasayan (s.d. fine-CHEM LTD BOISAR 401501, iron (metal) powder, electrolytic-300 mesh LR, Product No. 38601) and using a *Fritsch Planetary micromill 'Pulverisette 7'* high energy ball mill, the iron powder was milled for various durations. Inside the ball mill, bowls rotate on their own axes while simultaneously rotating through an arc around the central axis. The grinding balls and the material in the grinding bowl are thus acted upon by the centrifugal forces, which constantly change in direction and intensity, resulting in efficient, fast grinding process. The grinding bowl and the supporting disc rotate in opposite directions, so that the centrifugal forces alternately act in the same and opposite directions. This results in, as a frictional effect, the grinding balls running along the inner wall of the grinding bowl, and as an impact effect, the balls impacting against the opposite wall of the grinding bowl. The energy thus created by impact is many times higher than for traditional mills. This results in excellent grinding performance and considerably shorter grinding times. Atmospheric contamination is minimized by sealing the vial with a flexible 'O' ring after the powder has been loaded. A milling medium of toluene is used to avoid contamination from the milling tools and minimize the wear. The balls to powder ratio was maintained at 10:1.

2.2. Surface passivation

The ultrafine power was then coated with polyaniline (PANI) using an rf plasma polymerization technique [12]. This was carried out in a home-made set-up shown in figure 1. The radio frequency plasma polymerization set-up incorporates the deposition chamber, made up of a borosilicate glass tube about 0.5 m in length and 0.035 m in diameter. The set-up is evacuated to a pressure of about 10^{-2} Torr by using a vane type rotary pump with a pumping speed of 100 l min^{-1}. The amplified output of the rf oscillator is capacitively coupled to the discharge tube, by means of two copper foils wrapped around the glass tube. The glass chamber is placed vertically with the samples placed inside. The magnetic samples were then stirred using a magnetic stirrer.

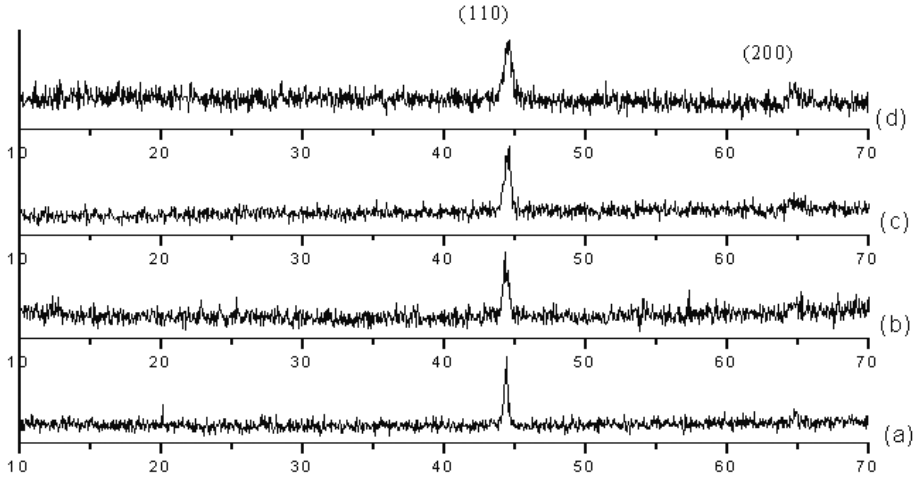

Figure 2. XRD patterns of iron samples at different milling time. (a) Fe as purchased (Fe). (b) Fe as purchased PANI coated (FePANI). (c) Fe 20 h milled uncoated (Fe20UC). (d) Fe 20 h milled PANI coated (Fe20PANI).

The magnetic sample inside the coating chamber is stirred by a magnetic stirrer placed below the chamber. The coating chamber and the magnetic stirrer are so placed that the magnetic field is uniform on all the particles. Thus when the stirrer rotates new grains are exposed to plasma each time inside the chamber. Since the iron particles are highly magnetic, even without using a stir bar (magnetic fish) in the chamber, particles move freely. Hence uniform surface modification of the particles is achieved.

The electrodes are so adjusted that they are well between the particles. The plasma is produced in between the electrodes and the monomer is sprayed into the plasma discharge through a vacuum stopcock and a needle valve. Inside the chamber the monomer gets polymerized and deposited on the nanoparticle surfaces stirred inside the bottom of the chamber. The surface of the nanoparticles can be continuously renewed and exposed to the plasma for polymer deposition during the plasma polymerization process.

Further, the powder was pressed into cylindrical discs of 13 mm diameter and around 1 mm thickness in a tempered steel die under a pressure of 7.5 tons.

3. Results and discussions

3.1. Structural analysis

The structural analysis and the identification of the phase were conducted with an x-ray diffractometer (Rigaku Dmax-C) using Cu Kα radiation ($\lambda = 1.5406$ Å) [13]. A scanning rate of 5° min^{-1} was applied in the 2θ range of 10°–70°. It is known that elemental iron exists in three phases. At room temperature, metallic iron exhibits a cubic ferromagnetic form (α-Fe) or a cubic paramagnetic form (γ-Fe). There exists another phase of iron, δ-Fe, which is not stable. The XRD analysis shown in figure 2 clearly indicates that the sample has body centred cubic structure (α-Fe JCPDS file No. C-85-1410). The samples are labelled as Fe, FePANI, Fe20UC and Fe20PANI for Fe as purchased, Fe as purchased PANI coated, Fe 20 h milled uncoated and Fe 20 h milled PANI coated respectively.

The x-ray diffraction patterns show two prominent peaks at $2\theta = 44.6°$ and 65.01°, corresponding to (110) and (200) planes respectively. Moreover as the milling time is increased the size of the particles is reduced which is evident from the XRD pattern. The grain size is estimated by employing the Debye–Scherrer formula $D = \frac{0.9\lambda}{\beta \cos\theta}$ where λ is the wavelength of the x-ray used, β is the FWHM of the XRD peak with maximum intensity and θ is the angle of diffraction. The lattice constant a is found from the relation $a = \frac{\lambda}{2\sin\theta}\sqrt{h^2+k^2+l^2}$. The particle size obtained from XRD for as purchased Fe is 23.1 nm while for 20 h milled Fe (Fe20UC) it is 15.6 nm. The lattice constant is found to be 0.287 nm. A core–shell structure can be proposed for the PANI coated samples with the core of the particles as metallic iron and the shell as PANI.

3.2. Morphology and size determination using TEM

A JOEL JEM 2200 FS electron microscope using an accelerating voltage of 200 kV was used to characterize the morphology and particle size distribution of nanoparticles. The TEM images, particle size distribution, HRTEM and EDS of Fe20PANI are shown in figures 3(a)–(d). The PANI coated Fe nanoparticles with spherical morphology are clearly seen. The average particle size was estimated to be 5.8 nm for Fe20PANI. The size distribution of Fe20PANI is between 2 and 14 nm. The EDS indicates the pure phase of α-Fe. The planes are identified from HRTEM. These have good correspondence with XRD results.

3.3. Magnetization studies using VSM

The room temperature magnetic properties were obtained from the hysteresis loops recorded in a vibration sample magnetometer model EG&G Par 4500. The experimental value of the saturation magnetization (M_s) for unmilled iron is in good agreement with the reported values [14]. The experimental value of M_s is found to be 15.91×10^5 A m^{-1} while that for the standard value is 17.45×10^5 A m^{-1}. The M_s values for the Fe and Fe20UC are 203.85 and 163.08 emu g^{-1} respectively, while the coercivities (H_c) are

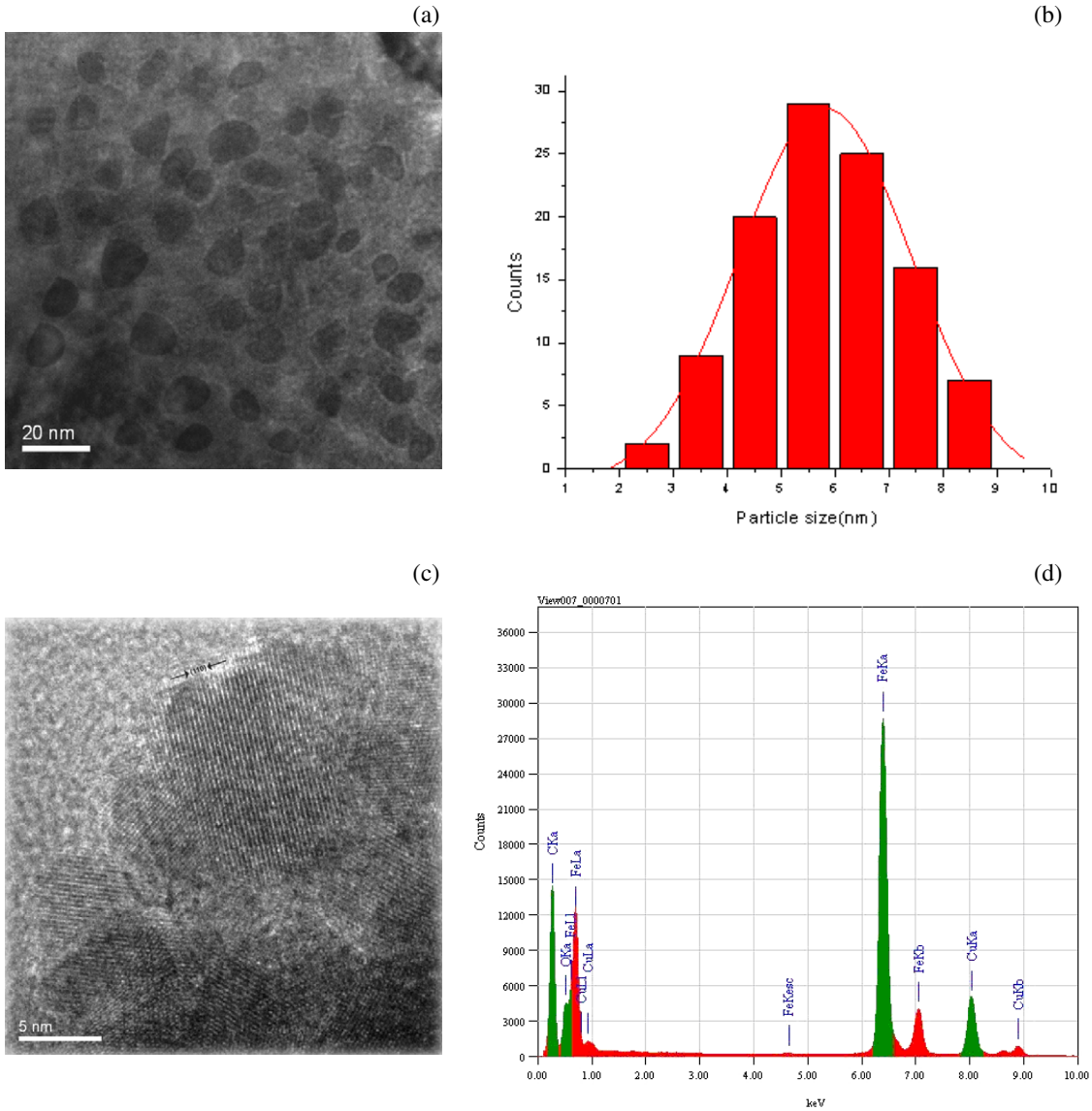

Figure 3. (a) Transmission electron micrograph of Fe20PANI. (b) Particle size distribution of Fe20PANI. (c) HRTEM of Fe20PANI. (d) EDS of Fe20PANI.

31.76 and 72.84 Oe respectively (shown in figure 4). The increase in H_c may be due to the internal strains produced during the attrition of particles using high energy ball milling. The magnetization values are almost the same for the coated samples (FePANI and Fe20PANI). The largest size reported for the superparamagnetic haematite particles is 41 nm [15], showing the typical value of critical particle size in oxide systems.

The magnetization curves show almost negligible remanence for all the samples showing their superparamagnetic nature [16]. Clearer evidence of superparamagnetism is obtained by fitting the magnetization curve with the Langevin function for which it is assumed that the individual grains are single crystals with the number of grains equal to the number of domains. Langevin curve fitting is carried out for Fe unmilled, 10 h milled and 20 h milled samples to probe into the effect of grain size on the superparamagnetic behaviour (figures 5(a)–(c)). From the graphs it is clear that on milling the size of the particles is reduced and they tend to attain superparamagnetic nature.

3.4. Conductivity studies

Substantial data on I–V characteristics, at different temperatures for different particle size, were generated. The I–V characteristics of Fe20 show nonlinear behaviour (figure 6), which was anomalous. They were reproducible and this confirms that the nonlinear property is exhibited by 20 h milled PANI coated Fe nanoparticles and this is a result of surface phenomena occurring at the interfaces. This could be explained using the existing critical path model (CPM) [17–19].

In the critical path model, G_{ij} is the conductance between any two localized sites (or two conducting grains) i and j. By taking a value of the conductance G and considering

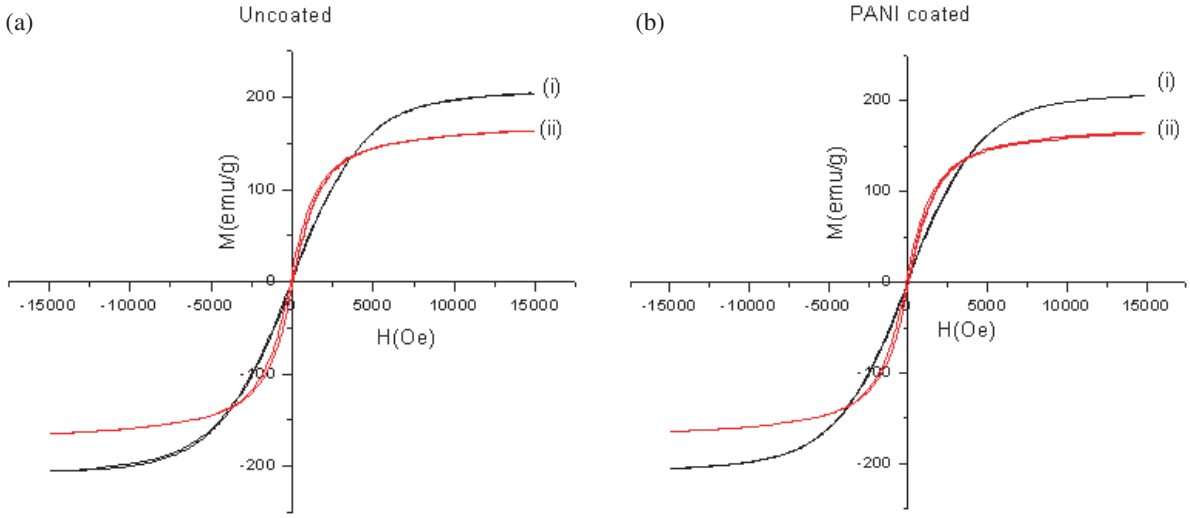

Figure 4. (a) Room temperature magnetization curves for (i) Fe, (ii) Fe20UC. (b) Room temperature magnetization curves for (i) FePANI, (ii) Fe20PANI.

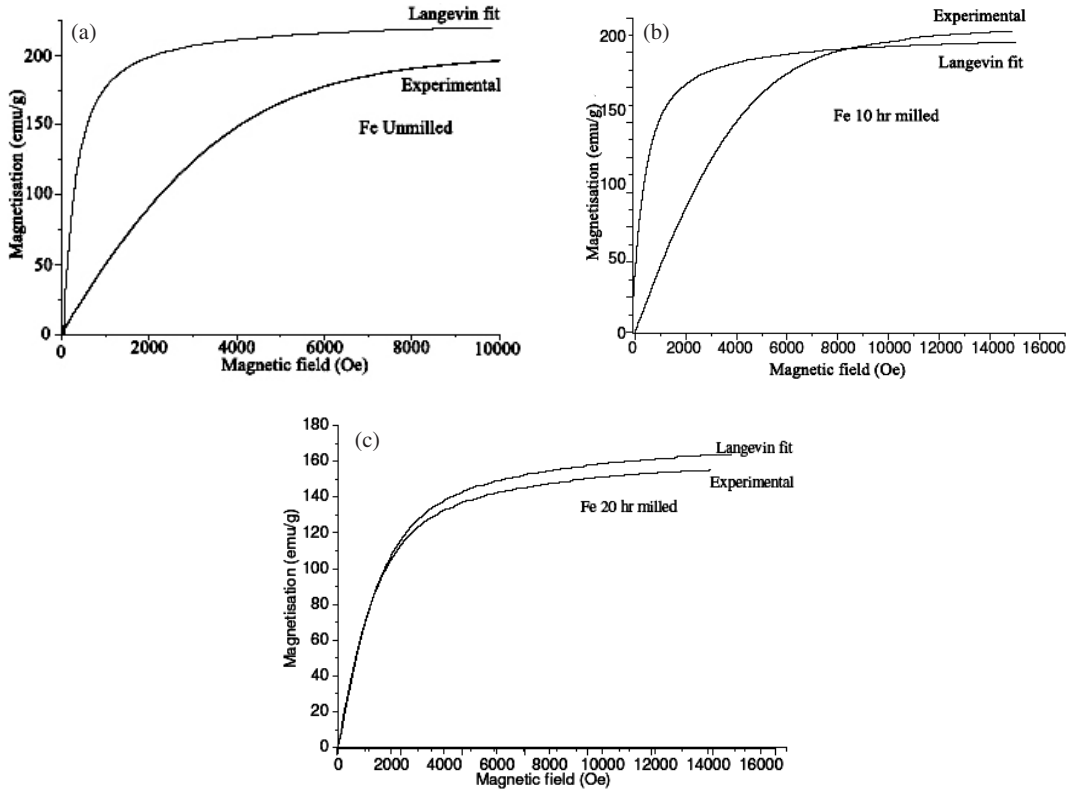

Figure 5. (a) Langevin fit for Fe. (b) Langevin fit for Fe10. (c) Langevin fit for Fe20.

any two sites as connected, if G is sufficiently large, the resulting connected sites will only form disjoint clusters. As G is lowered, the connected clusters are expected to increase in size until at $G = G_c$, the percolation conductance, an infinite network of connected sites is formed. Since G_c is the largest value of the conductance at which conduction over a continuous path is possible, it is identified as macroscopic conductance of the sample. Since the CPM deals with bond percolation, G_c is determined by the condition for bond percolation. In a d-dimensional system, there should be on average

$$b_c = \frac{d}{(d-1)} \tag{1}$$

allowed bonds per grain (site).

The electrical conduction in such systems results from the tunnelling of electrons and holes from charged grains to neutral

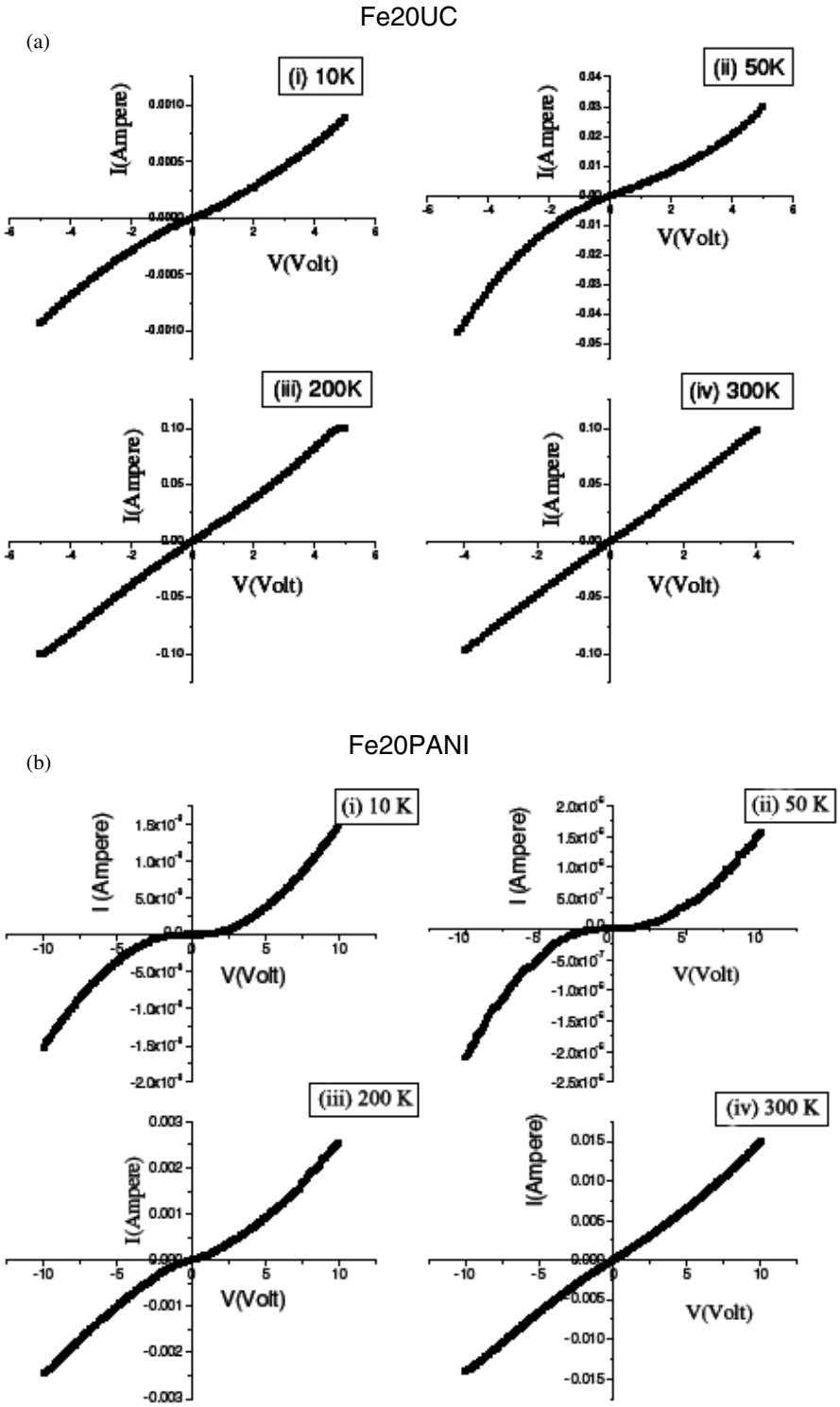

Figure 6. (a) I–V graph for Fe20UC at various temperatures: (i) 10 K, (ii) 50 K, (iii) 200 K, (iv) 300 K. (b) I–V graph for Fe20PANI at various temperatures: (i) 10 K, (ii) 50 K, (iii) 200 K, (iv) 300 K.

grains. To generate charge carriers, electrons have to be moved from one neutral grain to another. This process requires at least an energy $E_c = e^2/KD$ (eV), where e is the electronic charge, D is the grain size, and K is the dielectric constant of the inhomogeneous system. In the low field limit, the charge carriers are thermally activated. The conductance G_{ij} between two grains i and j is then

$$G_{ij} = G_0 \exp\left(-2\chi S_{ij} - E_{ij}/kT\right) \tag{2}$$

where χ is the WKB tunnelling constant.

Since the sizes of all the particles under consideration are not the same, a log normal distribution of the charging energy is taken. The log normal distribution for the size of grains,

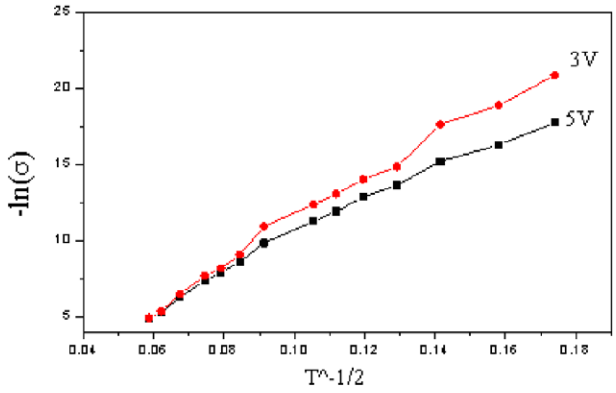

Figure 7. $-\ln\sigma$ versus $T^{-1/2}$ for voltages 3 and 5.

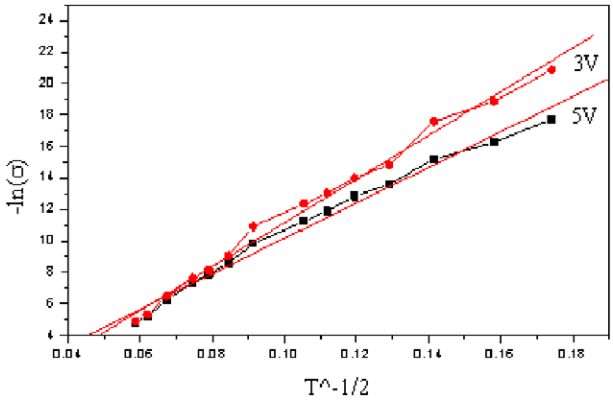

Figure 8. $-\ln\sigma$ versus $T^{-1/2}$. A linear fit of figure 7.

$P(E_c)$, will also be a log normal distribution [20]:

$$P(E_c) = \frac{1}{\sqrt{2\pi}}\frac{1}{\ln\mu}\exp\left\{-\frac{\left[\ln\frac{E_c}{E_0}\right]^2}{2(\ln\mu)^2}\right\}\frac{1}{E_c} \tag{3}$$

where μ is the parameter controlling the width of the distribution, and $E_0 = e^2/KD_0$ (eV) is the most probable value of E_c. Thus b_c will take the form

$$b_c = 8x\left\{\int_{-1}^{1} de_i\rho(|e_i|kTY/E_0)\int_{-1}^{1} de_j\rho(|e_j|kTY/E_0) \times\left[\left(\frac{sYE_0}{2C_0(x)}+1\right)^3-1\right]\right\}\left\{\int_{-1}^{1} de_i\rho(|e_i|kTY/E_0)\right\}^{-1}. \tag{4}$$

Here

$$Y = \ln\left(\frac{G_0}{G_c}\right)$$
$$x = ND_0^3\frac{\pi\sqrt{2}}{6} \tag{5}$$

(for body centred cubic) is the volume fraction of the conducting grain (metal volume fraction).

$$s = [1-\tfrac{1}{2}(|e_i|+|e_j|+|e_i-e_j|)]\Theta_{(s)}$$
$$C_0(x) = e^2\chi/K = \frac{\eta\left[(\pi/6x)^{1/3}-1\right]}{(\pi/6x)^{1/3}-0.5} \tag{6}$$

where

$$\eta = e^2\chi/\varepsilon, \tag{7}$$

ε being the dielectric constant of the insulator; absolute values of e_i and e_j are taken because of taking the symmetry of positively charged and negatively charged grains. In the case of $d = 3$, $b_c = 1.5$ (using equation (1)) [21] and also taking $\eta = 3.8$ eV [22], $\Delta^* \sim 1$ meV, $\rho_0 = \frac{0.1}{\Delta^*}$ and $E_0 \sim 20$ meV ($\sim$150 Å grains, which is found to be the maximum particle size from the TEM and XRD results), the theoretical plots of the calculated Y as a function of T and x for two values of μ were produced. If we select a particular value for μ, we get that $-\ln\sigma$ behaves as $(T^{-1/2})$ [17]. It can be seen that the I–V curves of unmilled Fe samples display linear characteristics typical of metal systems while milled coated

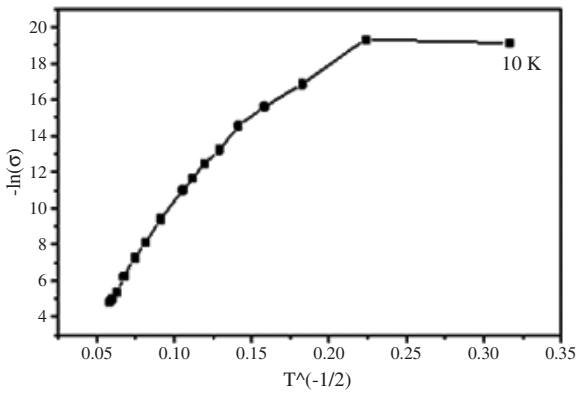

Figure 9. $-\ln\sigma$ versus $T^{-1/2}$ at 5.8 V for Fe20PANI.

samples of Fe display a nonlinearity even at room temperature. This nonlinear I–V plot is the resultant of the intergranular transition when the metal volume fraction falls below a critical value. Using the formula $x = ND_0^3\frac{\pi\sqrt{2}}{6}$, the metal volume fraction is calculated for Fe which is bcc and it is found to be about 0.713.

4. Model fitting

Figures 7–9 show the fitting of the model with the above-proposed model. Figure 8 shows a linear fit of figure 7 obeying the relation $-\ln\sigma \propto T^{-1/2}$. However, figure 9 shows a deviation from this linear fit at $T = 10$ K, which is the minimum temperature beyond which the model is no longer valid. A sudden change in the $-\ln\sigma$ versus $T^{-1/2}$ at 10 K gives a minimum temperature limit for the model.

The dependence of the conductivity on the voltage variation is also shown. This variation is similar to the variation of the metallic volume fraction as shown in the model. This is due to the fact that as voltage increases more and more electrons get enough charging energy to hop through the barrier and in effect increase the current. This relation is found to be valid up to 300 °K. Above room temperature the study did not yield good results because the polymer coating thermally diffused and the system behaved like bulk.

As a further confirmation of the model, slope of the linear $-\ln\sigma$ versus $T^{-1/2}$ curve is drawn (figure 10). This is in

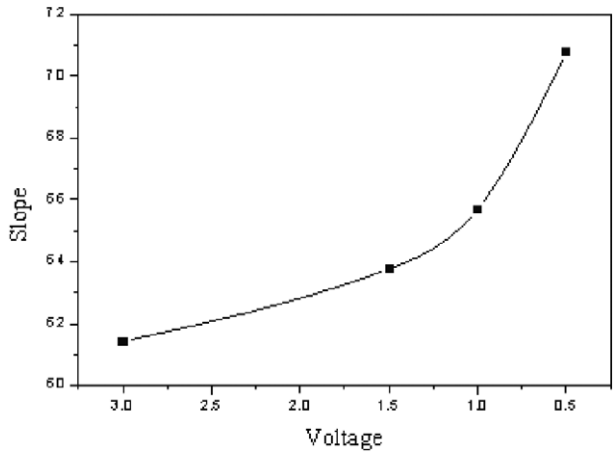

Figure 10. Voltage slope of the linear $-\ln\sigma$ versus $T^{-1/2}$ curve.

exact agreement with results reported earlier [21]. This is also evidence for the intergranular electronic transfer in these systems.

5. Conclusion

HEBM was successfully used to reduce the particle size considerably (relative reduction of 32%). The anomalous result for I–V curves was explained by the critical path model. The conductivity has a temperature dependence of the form $-\ln\sigma \propto T^{-1/2}$ for a wide range of temperature (10 to 300 K). It is observed that in the case of Fe–PANI nanocomposites the nonlinearity is observed up to a temperature of 10 K. This theory will be valid only when the critical volume fraction is less than a critical value.

As far as applications are concerned, surface coating of nanoparticles not only provides passivation, but also the reduced conductivity together with passivation can be used for transformer core applications. If one works out the eddy current losses of these nanomaterials coated with various polymers, this can be a useful material and has a definite advantage over conventional Fe cores. If the composite can be tailored to exhibit nonlinear (I–V) behaviour at room temperature, this can be thought of as a varistor [23].

Acknowledgments

This research work was supported by the Department of Science and Technology (File No. SP/S2/M-64/96), Kerala State Council for Science, Technology and Environment (File No. 079/SRSPS/2004/CSTE and D.O. No. 004/FSHP/05/KSCSTE) and the All India Council for Technical Education (File No. 8023/RID/RPS-73/2004-05).

References

[1] Bødker F, Mørup S and Linderoth S 1994 *Phys. Rev. Lett.* **72** 282
[2] Del Bianco L, Hernando A, Navarro E and Bonetti E 1998 *J. Magn. Magn. Mater.* **177** 939
[3] Carpenter E E 2001 *J. Magn. Magn. Mater.* **225** 17–20
[4] Banerjee S, Roy S, Chen J W and Chakravorty D 2000 *J. Magn. Magn. Mater.* **219** 45–52
[5] Humfeld K D, Giri A K, Majetich S A and Venturini E L 2001 *IEEE Trans. Magn.* **37** 2194–6
[6] Nalwa H S 2002 *Nanostructured Materials and Nanotechnology* (New York: Academic) pp 2–23
[7] Koch C C 2003 *Rev. Adv. Mater. Sci.* **5** 91–9
[8] Yu X B, Dou T, Wu Z, Xia B J and Shen J 2006 *Nanotechnology* **17** 268–71
[9] Geng D-Y, Zhang Z-D, Liu W, Zhao X-G, Yu M-H, Ren W-J, Xiao Q-F, Grossinger R and Hauser R 2003 *J. Phys. D: Appl. Phys.* **36** 375–9
[10] Srikanth H, Hajndl R, Chirinos C and Sanders J 2001 *Appl. Phys. Lett.* **79** 3503
[11] Yavuz O, Ram M K, Aldissi M, Poddar P and Hariharan S 2005 *J. Mater. Chem.* **15** 810–7
[12] Shi D, Wang S X, van Ooij W J, Wang L M, Zhao J and Yu Z 2001 *Appl. Phys. Lett.* **78** 1243–5
[13] Suryanarayana C and Grant Norton M 1998 *X-Ray Diffraction* (New York: Plenum) pp 98–100, 212–13
[14] Cullity B D 1978 *Introduction to Magnetic Materials* (Reading, MA: Addison–Wesley) chapter 4
[15] Raming T P, Winnubst A J A, van Kats C M and Philipse A P 2002 *J. Colloid Interface Sci.* **249** 346–50
[16] Kittel C 1946 *Phys. Rev.* **70** 965
[17] Mott N F 1969 *Phil. Mag.* **19** 835
[18] Sheng P and Klafter J 1983 *Phys. Rev.* B **27** 2583
[19] Abeles B, Pinch H L and Gittleman J I 1975 *Phys. Rev. Lett.* **35** 247
[20] Granquist C G and Buhrman R A 1976 *J. Appl. Phys.* **47** 2200
[21] Shante V K 1977 *Phys. Rev.* B **16** 2597
[22] Hafeli U O and Pauer G J 1999 *J. Magn. Magn. Mater.* **194** 76–82
[23] Lauf R J and Bond W 1984 *Ceram. Bull.* **63** 278–81